31st Annual International Conference of the IEEE EMBS
Minneapolis, Minnesota, USA, September 2-6, 2009

Singular Value Decomposition-based Analysis on Fluorescence Molecular Tomography in the Mouse Atlas

Zhun Xu, Xiaolei Song, Jing Bai, *Fellow, IEEE*

***Abstract*—The application of CCD camera improves the quality of fluorescence molecular tomography (FMT). However, large size of data set offered by CCD might increase the computational burden in the reconstruction. To balance the data size and reconstruction quality, singular value decomposition (SVD)-based analysis is applied. Simulation is performed with mouse atlas. By observing the relative gain of number of effective SVD components and reconstruction results, we find that the minimum field of view can be obtained for each projection in order to realize the optimization of experimental setup and furthest utilize data set.**

I. Introduction

Fluorescence molecular tomography (FMT) is applied to probing the distribution of fluorescence reporters associated with cellular functions and offering three-dimensional quantitative visualization of those reporters in vivo in small animals [1]-[3]. It is the critical stage in 2007 during the development of FMT imaging system when the implementation of free-space fluorescence tomography in the 360° geometry with CCD-camera-based detection was proposed, making it possible to yield a superior information content data set [2].

Along with the superior information content available in the measurements brought by the 360° CCD camera based FMT system, an important issue that should be considered is how to deal with the vast amount of data. When considering the size of the CCD measurement (512×512) and the number of projections (5-100), there will be typically 10^6-10^8 measurements. In the linear scheme of diffusion equation, solving the matrix equation in such order of magnitude requires very high memory and computational ability of the computers. And the question is, do we really need all these measurements for the reconstruction? To answer this question, numerical analysis is required to optimize the experimental parameters, fully utilize the information of measurements, avoid information abundant, and achieve the practical computation scheme in the reconstruction.

Similar research has been done before. Culver *et al*. [4] firstly employed singular-value analysis (SVA) to analytically estimate the optimal experimental parameter in 2001. Graves *et al*. [5] also applied this tool into optimizing source/detector arrangements and field of view in parallel plate geometries. And Lasser *et al*. [6] in 2007 used SVA to optimize experimental parameters in 360° FMT, including the projection number, illumination style, spatial sampling and the field of view. Herein we focus on the optimal field of view for detector and the projection number in the mouse atlas. To our knowledge, it is the first time that such optimization is applied into the mouse atlas. And different from previous study, the analysis is based on the finite element method (FEM) instead of analytical formula based on born approximation. Besides, both the Fourier coefficients and singular values are considered in our analysis. Since the nature of reconstruction is ill-posed matrix inversion, such analysis is necessary also from the perspective of reconstruction.

II. Methodology

A. Forward problem discription

In a continuous wave (CW) FMT experiment, the model of photon propagation can be simplified as the diffusion theory [7].

The coupled diffusion equations are given by

$$\nabla \cdot [D_x(r)\nabla\Phi_x(r)] - \mu_{ax}(r)\Phi_x(r) = -\Theta_s\delta(r - r_{sl}) \quad (1)$$

$$\nabla \cdot [D_m(r)\nabla\Phi_m(r)] - \mu_{am}(r)\Phi_m(r) = -\Phi_x(r)\eta(r)\mu_{af}(r) \quad (2)$$

where r is the position vector, $\Phi_x(r)$ and $\Phi_m(r)$ represent the excitation and emission photon intensity (photons/cm^2/s) at position r respectively, $\mu_{ax,m}$ is the total absorption coefficient at the respective wavelengths, and $D_{x,m}$ is the optical diffusion coefficient equivalent to $1/3(\mu_{ax,m} + \mu'_{sx,m})$,where $\mu'_{sx,m}$ is the reduced scattering coefficient (cm^{-1}). $\eta(r)$ is the fluorophore's quantum efficiency and μ_{af} is the absorption coefficient due to

Manuscript received April 5, 2009. This work is supported by the National Nature Science Foundation of China (No.30670577, 60831003), the Tsinghua-Yue-Yuen Medical Science Foundation, the National Basic Research Program of China (No.2006CB705700), the National High-Tech Research and Development Program of China (No.2006AA020803)，and China Postdoctoral Science Foundation Funded Project (No. 20080440391).

Jing Bai is with School of Medicine, Tsinghua University, Beijing, 100084, P.R.China (corresponding author to provide phone: 86-10-62786480; fax: 86-10-62780650; e-mail: deabj@tsinghua.edu.cn).

Zhun Xu is with School of Medicine, Tsinghua University, Beijing, 100084, P.R.China. (e-mail: zhun310@yahoo.com.cn).

Xiaolei Song is with School of Medicine, Tsinghua University, Beijing, 100084, P.R.China. (e-mail: lisasonger@gmail.com).

fluorophores (cm^{-1}), which is directly proportional to the fluorophore concentration. r_{sl} ($l = 1, 2, ...L$) represents the different excitation point source positions with respect to the subject with the amplitude Θ_s .The coupled diffusion equations are supplemented by the Robin-type boundary conditions on the boundary [8], [9].

FEM is used to assemble the stiffness matrices of (1) and (2). Combining the matrix transformation [10] and free-space light propagation [11], the reconstruction problem of FMT is converted into the matrix equation of $Wx = b$ where elements of b is the values on the corresponding boundary finite element nodes mapped from the measurements on the CCD, W is the weight matrix, and the elements of vector x correspond to the fluorophore values on each nodes.

B. Singular value decomposition-based analysis

Considering the singular-value decomposition (SVD) [12] of $W \in R^{m \times n}$, it can be written in the form:

$$W = \sum_{i=1}^{n} u_i \sigma_i v_i^T$$

where $U = (u_1, ..., u_n) \in R^{m \times n}$ and $V = (v_1, ..., v_n) \in R^{n \times n}$ are matrices with orthonormal columns. And the solution of the matrix equation comes to

$$x = \sum_{i=1}^{n} \frac{u_i^T b}{\sigma_i} v_i \qquad (3)$$

If b consists of the noise e with Gaussian distribution, i.e., $b = b_{exact} + e$,and matrix W also consists the noise part E , satisfying $W = W^{exact} + E$,where the elements of vector e and matrix E are both normally distributed with zero mean, and standard deviations of them are δ_1 , δ_2 respectively. Then the expected value of $\left| u_i^T e \right|$ is δ_1 , and the expected value of $\left\| E \right\|_2$ is approximately $\delta_2 \sqrt{m}$ [13]. As a consequence, we cannot resolve the component of x_{exact} ($W^{exact} x_{exact} = b_{exact}$) from the noise when $\left| u_i^T b \right| \le \delta_1$ or $\sigma_i \le \delta_2$. So the corresponding coefficient in (3) should be omitted in the reconstruction process. Specifically, when $0 < \left| u_i^T b \right| - \delta_1 < \varepsilon$ and $\sigma_i - \delta_2 > \varepsilon$, the measurement errors dominate and the ith component of equation (3) turns to $v_i \delta_1 / \sigma_i$; when $\left| u_i^T b \right| - \delta_1 > \varepsilon$ and $0 < \sigma_i - \delta_2 < \varepsilon$, the matrix errors dominate and the ith component of (3) becomes $(u_i^T b / \delta_2) v_i$. Here ε is the small value with its order approximate to δ_1 and δ_2 . Those components that are not eliminated as the noise are defined as effective SVD components.

III. Simulations

Simulations are carried out in Matlab 7.4 on a personal computer with 1.5GHz Pentium 4 processor and 1 GB RAM. COMSOL Multiphysics 3.3 is applied to obtain the FEM stiffness matrix for the further matrix computing.

A. Experimental setup

The experimental system of free-space 360° FMT projections is shown in Fig. 1(a). Our investigation is implemented in the same abdomen part of 3-D mouse atlas as Song et al.'s work [14].Optical parameters were assigned as μ_a . $0.12\ mm^{-1}$ and μ_s' . $1.2\ mm^{-1}$ inside the kidneys (the red part in Fig. 1(c)), and μ_a . $0.23\ mm^{-1}$ and μ_s' . $1.0\ mm^{-1}$ outside the kidneys. The excitation light is modeled as an isotropic point source that locates one mean free path of photon transport beneath the surface. The rotational axis of the mouse is defined as the z axis that passes the center point in Fig. 1 (b). p illumination positions in the simulation are corresponding to p projections with the CCD capture at $360/p$ degrees. Fig. 1(b) is the sketch figure that shows 15 illumination positions for projections in the view of transect. The field of view (FOV) for the detection with respect to one particular excitation source is also shown in the figure. Dual fluorophore targets are embedded in the mouse (Fig. 1 (d)), and the targets are set to point sources. The geometry of the mouse abdomen part is discretized into 1294 nodes and 5127 tetrahedral elements with FEM. In this study, 6, 8, 10, 15, projections are investigated respectively with the same finite element mesh discretization. Here we neglect the error in the mapping from CCD measurements to the corresponding surface measurements and assume that the system error that impacts the surface mesh values is normally distributed. Thus 10% Gaussian noises are added to the surface measurements, i.e. , $\delta_1 = \left\| e \right\|_2 / \sqrt{m} = 0.1 \left\| b \right\|_2 / \sqrt{m}$., and let $\delta_1 = \delta_2$.

B. Results

Fig. 2 shows number of the effective SVD components (NESC) as a function of the FOV with different projections. It can be observed that there is a significant increase of NESC when the FOV increases from 30° to 60° . However, further increase of FOV, especially when it is larger than 90° ,does not yield a corresponding relative gain in NESC. When the FOV increases from 180° to 210° , the NESC decreases. As the number of projection increases, such trend of NESC is more evident. Yet it is observed that the gain is strong when

the number of projections increases. Due to the irregular boundary shape of the mouse, it requires as many projections as possible to offer complete information for the reconstruction. Simulations with more projections are not implemented due to the limitation of computational capacity. However, it can be inferred that increasing the projections would yield a corresponding gain in NESC.

As a complementary study to the SVD analysis,

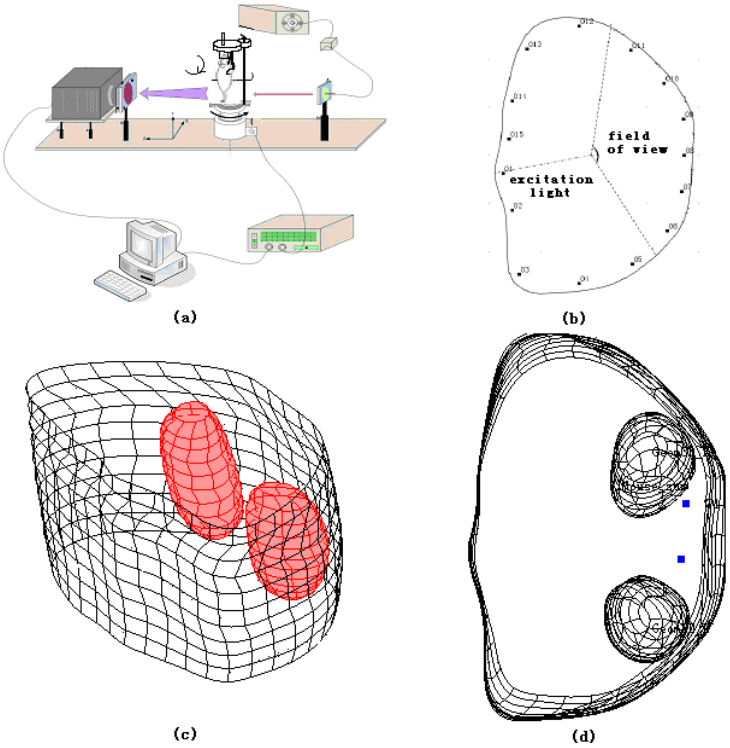

Fig. 1. Experimental setup and the geometrical model of a mouse abdomen part. (a) the sketch of free-space FMT experimental setup, which is similar to [2], (b) the sketch that shows 15 illumination positions for projections in the view of transect, (c) the mouse geometry model used for reconstruction, (d) another view of the mouse geometry model with dual fluorescence targets (point sources) within the body.

reconstructions using (3) with effective SVD components are also performed. Results indicate that the targets can be positioned well with the FOV that yields largest NESC. However, when the number of projection is small, it fails to resolve the two targets (Fig .3 (a)-(d)). And with 15 projections there is no significant difference of reconstruction results between the FOV of 90° and 180° . Besides, the error reconstructed fluorescence yields of two targets is getting smaller when the number of projections increases (the true fluorescence yields are set to 1), but does not change a lot when FOV increased under the given number of projections. Therefore, it can be regarded that 15 projections with FOV of 90 ° is the optimal experimental setup among all the parameters we investigate based on the computational ability.

IV. DISCUSSION

In this study, SVD-based analysis is used in FMT, trying to reduce the computational burden in reconstruction. Different from the reconstruction in the phantom with the simple and symmetrical geometry, reconstruction in the small animal experiment is much more complicated due to the complex boundaries, which requires more nodes and elements in FEM mesh generations. The method we adopt in this study is helpful in the experiment to optimize the scale of measurement.

For the (m.n) matrix W , the maximum number of effective component is min(m,n). According to the mesh discretization in our simulation, this value is 1294. However, due to the ill-posedness of matrix, not all the SVD components are required for the reconstruction. In this study, a possible strategy is proposed to determine how to treat the SVD components in FMT reconstruction problem. Results suggest that the data size cannot be reduced by decrease the number of projections, but by the decrease of FOV. Since several regularization-based reconstruction algorithms are aimed to handle those components that might be noise [15], it is more computationally practical to apply those iteration-based algorithms into reconstruction after the realization of optimization by SVD-based analysis in order to improve the computational efficiency.

Future work might include the optimal illumination positions in the small animal experiment in order to increase the number of effective SVD components. And of more importance, the method is planned to apply into real experiment.

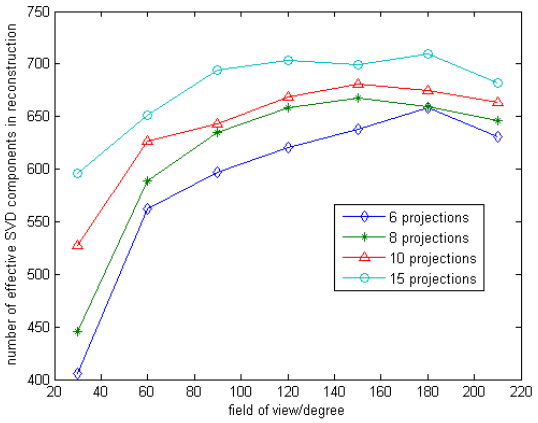

Fig. 2. The effective SVD components as a function of the FOV with different projections.

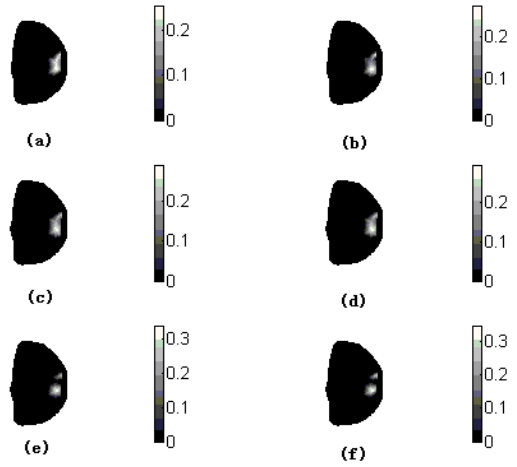

Fig. 3. Reconstruction results in the view of 2D transects. (a) 6 projections with FOV of 180° ,(b)8 projections with FOV of 150 ° ,(c)10 projections with FOV of 120° ,(d) 10 projections with FOV of 150° ,(e) 15 projections with FOV of 90° ,(f) 15 projections with FOV of 180° .The colorbar represents the reconstructed fluorescence yields

ACKNOWLEDGMENT

This work is supported by the National Nature Science Foundation of China (No.30670577, 60831003), the Tsinghua-Yue-Yuen Medical Science Foundation, the National Basic Research Program of China (No.2006CB705700), the National High-Tech Research and Development Program of China (No.2006AA020803), and China Postdoctoral Science Foundation Funded Project (No. 20080440391).

REFERENCES

[1] V. Ntziachristos, "Fluorescence molecular imaging," *Annu. Rev. Biomed. Eng.*, vol. 8, pp. 1-33, 2006.

[2] N. Deliolanis, T. Lasser, D. Hyde, A. Soubret, J. Ripoll. and V. Ntziachristos, "Free-space fluorescence molecular tomography utilizing 360° geometry projections," *Opt. Lett.*, vol. 32, pp. 382-384 ,2007.

[3] E. E. Graves, R. Weissleder and V. Ntziachristos, "Fluorescence molecular imaging of small animal tumor models," *Curr. Mol. Med.*, vol. 4, pp. 419-430, 2004.

[4] J. Culver, V. Ntziachristos, M. Holboke and A. Yodh, "Optimization of optode arrangements for diffuse optical tomography: a singular value analysis," *Opt. Lett.*, vol. 26, pp.701-703, 2001.

[5] E. Graves, J. Culver, J. Ripoll, R. Weissleder and V. Ntziachristos, "Singular value analysis and optimization of experimental parameters in fluorescence molecular tomography," *J. Opt. Soc. Am. A.*, vol.21, pp. 231-241, 2004.

[6] T. Lasser and V. Ntziachristos, "Optimization of 360° projection fluorescence molecular tomography," *Med. Imag. Analysis.*, vol. 11, pp. 389-399, 2007.

[7] A. Cong and G. Wang, "A finite-element-based reconstruction method for 3D fluorescence tomography," *Opt. Express.*, vol. 13, pp. 9847-9857, 2005.

[8] R. C. Haskell, L. O. Svaasand, T. T. Tsay, T. C. Feng, M. S. McAdams and B. J. Tromberg, "Boundary conditions for the diffusion equation in radiative transfer," *J. Opt. Soc. Am. A.*, vol. 11,pp. 2727-2741, 1994.

[9] M. Schweiger, S. R. Arridge, M. Hirauka and D. T. Delpy, "The finite element method for the propagation of light in scattering media: Boundary and source conditions," *Med. Phys.*, vol. 22, pp. 1779-1792, 1995.

[10] Z. Xu and J. Bai, "Analysis of finite-element-based methods for reducing the ill-posedness in the reconstruction of fluorescence molecular tomography," *Prog. In Nat. Sci.*, vol. 19, pp. 501-509, 2009.

[11] J. Yao, G. Hu and J. Bai, "Modeling and validation of light propagation in free space for non-contact near-infrared fluorescence tomography," *J. Infrared Millim. Waves*., Vol. 27, 2008

[12] W. H. Press, B.P.Flannery, S.A.Teukolsky and W.T.Vetterling, *Singular Value Decomposition. In: Numerical Recipes in FORTRAN: The Art of Scientific Computing*. Cambridge University Press, Cambridge, 1992.

[13] M. Hanke and P.C.Hansen, "Regularization methods for large-scale problems," *Surveys Math. Indust.*, vol. 3, pp. 253-315, 1993.

[14] X. Song, D. Wang, N. Chen, J. Bai and H. Wang, "Reconstruction for free-space fluorescence tomography using a novel hybrid adaptive finite element algorithm," Opt. Express., vol. 15, pp.18300-18317, 2007.

[15] P.C.Hansen, Rank-Deficient and Discrete Ill-posed Problems, SIAM Press, pp.135-173, 1998.